Activation Mechanism of Nickel(0) *N*-Heterocyclic Carbene Catalysts Stabilized by Fumarate Ligands

Michael T. Robo, Amie R. Frank, Ellen Butler, Alex J. Nett, Santiago Cañellas, Paul M. Zimmerman,* and John Montgomery*

Department of Chemistry, University of Michigan, Ann Arbor, MI 48109-1055, USA

Abstract: Nickel(0) catalysts of *N*-heterocyclic carbenes (NHCs) that are stabilized by electronic deficient alkenes possess desirable properties of air tolerance and ease of handling while also retaining high catalytic activities. Since catalyst stability often comes at the expense of catalytic activity, we have undertaken a detailed study of the activation mechanism of a new IMes-nickel(0) catalyst stabilized by di-(*o*-tolyl) fumarate that converts the stable pre-catalyst form into a catalytically active species. Computational evaluation provided evidence against a simple ligand exchange as the activation mechanism, and a stoichiometric activation process that covalently modifies the stabilizing ligand was identified. A detailed computational picture for the activation process was developed, with predictive insights that explain the catalyst features that lead to both active and inactive precatalysts.

Introduction

A vast array of synthetic methods involving nickel catalysis has been developed in recent years.[1] Methods that involve exogeneous reductants often are best accomplished with air-stable Ni(II) catalysts,[1d,1e] which are desirable compared with more air-sensitive Ni(0) counterparts. While processes involving phosphine and pyridine ligand frameworks often perform well with Ni(II) precursors,[2] reactions that involve *N*-heterocyclic carbene ligands are more commonly performed with $Ni(COD)_2$ as the precatalyst. This choice is due to inefficiencies in the catalyst reduction and formation of catalytically active Ni(0) species. At the same time, *in situ* formation of Ni(0)-NHC complexes has disadvantages of instability of

Ni(0) precatalysts and NHC ligands,[3] inhibitory effects of cyclooctadiene in some classes of catalytic processes, especially C-H activation processes involving LLHT activation mechanisms,[4] and the precise control of metal-ligand stoichiometry, especially on the small scales required for high throughput experimentation.[5]

Ni(0) catalysts that are stabilized by simple alkenes have proven effective across many reaction classes, with more electron-deficient alkenes typically providing more stable but less active catalysts compared with the most commonly employed precursors such as $Ni(COD)_2$. Catalyst **1**, initially reported by Cavell,[6] includes IMes as the NHC ligand and dimethyl fumarate as the stabilizing π-acid and serves as a prototypical example of the increased stability and diminished reactivity imparted by the electron-deficient alkene additives. Recent work from our lab built upon this template and examined acrylate, fumarate, and methacrylate π-acids to refine the stability-reactivity balance.[7] While catalyst **1** possesses exceptional stability in air and performs effectively in the oxidation of secondary alcohols,[8] we found that C-C bond-forming processes including aldehyde-alkyne reductive couplings and Buchwald Hartwig aminations were not effective due to deactivation of the catalyst by the fumarate. Systematic variation of the NHC and stabilizing π-acid led to the identification of a number of catalysts that participate effectively with these reaction classes and rapidly initiate without a discernable induction period. Our initial observations found that the optimal π-acid depends on the NHC ligand, and the stability-reactivity continuum can be optimized according to the precise catalytic properties and stability desired. Complexes **2**-**4** were found to display excellent catalytic properties in aldehyde-alkyne reductive couplings (catalysts **2** and **3**) and Buchwald-Hartwig aminations (catalyst **4**) and are now sold by commercial vendors (Figure 1).

Other classes of promising air-stable Ni(0) catalysts have subsequently been disclosed by Cornella and Engle, with Ni(0) centers stabilized by either stilbene or quinone π-acids.[9] These catalysts possess the advantage of enabling modular *in situ* coordination to different ligands, whereas the NHC/π-acid combinations have the advantage of being a single-component system with pre-defined structure and metal-ligand stoichiometry, as illustrated with electronic-deficient akenes[3,7] and other olefin classes.[4,10] We

envision that the latter characteristics will offer unique advantages with NHC catalysts in high-throughput arrayed methods where inefficient mixing and imprecise control of metal-ligand stoichiometry are avoided with a single-component, well-defined catalyst source.

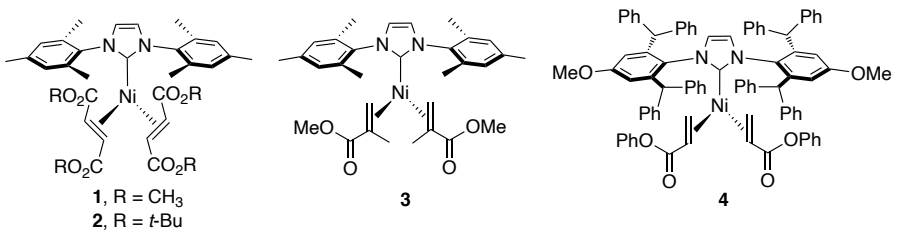

Figure 1. First generation stable Ni(0) NHC complexes. CAS numbers: **2**: 2230140-59-5, **3**: 2230140-51-7, **4**: 2230140-52-8.

Prior studies from numerous laboratories have illustrated that judicious choice of alkene ligands can play a key role in tuning the stability and reactivity of numerous families of Ni(0) catalysts, a current gap in the field is the understanding of how Ni(0) complexes stabilized by simple ligands undergo activation to more active forms of the catalyst. A question that remains unanswered for most Ni(0) precatalysts is whether simple ligand dissociation affords active catalyst forms, or if more complex activation steps involving chemical modification of the alkene are required. We have now studied this question in detail with new fumarate catalysts that build on the design features of an NHC ligand paired with a π-acid selected to balance stability and reactivity. In this study, the fate of the stabilizing alkene ligand and mechanism of catalyst activation are elucidated through experimental and computational studies that evaluated different mechanisms for catalyst activation, including displacement as well as covalent sequestration of the stabilizing π-acid.

Results and Discussion

Our initial report described the activity of catalysts **2-4** among other nickel(0) NHC complexes stabilized by electron-deficient alkenes and suggested that the stability-reactivity continuum could be tuned

to achieve desired catalyst properties.[7] In particular, fumarates with especially high binding affinity to nickel are expected to stabilize the resulting complex, but likely inhibit productive catalysis. Conversely, weakly bound fumarates would lead to unstable precatalysts, which would degrade prior to use in catalysis. When framed in this way, the thermodynamic affinity of fumarate to nickel takes a central role and leads to a key initial hypothesis: ligand exchange governs the stability-reactivity continuum for these precatalysts. In order to test this hypothesis and use this information to improve this family of catalysts, we set out to better understand the chemical principles that govern the relationship of stability and reactivity. The design strategy, based on this thermodynamic rationale, was to tune the fumarate binding affinity to offset the innate electronic stabilization of the electron-deficient alkene by steric interactions with the NHC. Specifically, we wanted to locate a region in chemical space where the fumarate ligand would be bound loosely enough to allow for reactivity, but also be bound strongly enough to maintain air-stability.

Evaluating the Thermodynamic Dissociation Hypothesis

To test whether the thermodynamics of ligand binding were controlling the activation of the Ni(0) NHC complexes, seven different fumarate complexes of IMes (**1-2**, **5-10**, Figure 2) with varying electronics and sterics were considered. In the model reaction of 4-fluorobenzaldehyde (**12**) and phenyl propyne (**13**) using triethylsilane as the reductant, a potential first step for activation of the Ni complex is displacement of the two fumarate ligands with aldehyde and alkyne. We computed the free energy of fumarate ligand exchange with the aldehyde and alkyne reaction components using seven representative fumarate complexes and compared their binding affinities to Cavell's original complex (**1**) (Table 1). Complex **1** was chosen as a reference point for this series, as it is known to be air-stable and was observed to be unreactive in the reductive couplings of aldehydes and alkynes and in Buchwald Hartwig aminations.[7] We anticipated that if the mechanism of catalyst activation simply involves exchange of the fumarate **16** for the aldehyde and alkyne components (**12** and **13**), then the catalysts with lowest free energy of exchange will most easily reach the active catalyst state. As seen in Table 1, the complexes examined were found to have similar or higher fumarate binding affinities, relative to **1**, with the exception of di-(*t*-butyl) fumarate complex **2**.

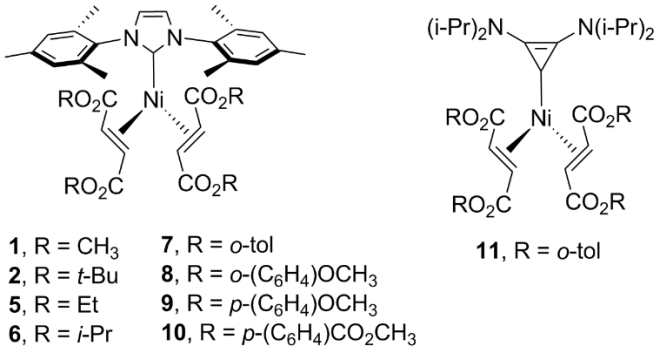

Figure 2. Catalyst structures used in this study

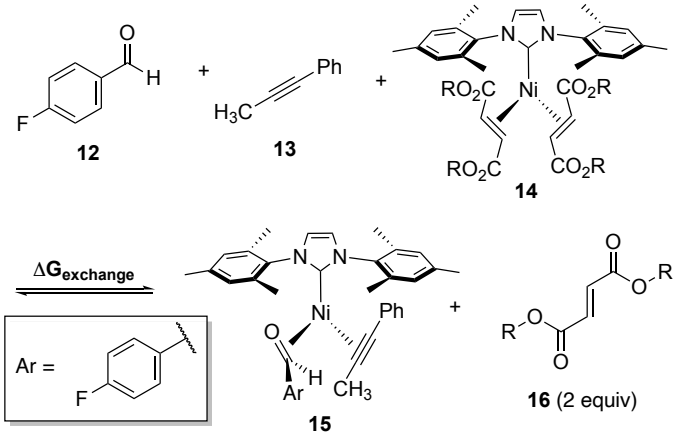

Catalyst	R group	ΔG exchange relative to 1 (kcal/mol)
1	Me	0.0 (reference)
2	*t*-Bu	-6.0
5	Et	-1.7
6	*i*-Pr	-0.5
7	*o*-tol	14.4
8	*o*-(C_6H_4)OCH_3	8.3
9	*p*-(C_6H_4)OCH_3	10.2
10	*p*-(C_6H_4)CO_2CH_3	12.3

Table 1. Computed free energy of ligand exchange. Free energies are calculated from ωB97X-D3/cc-pVTZ/THF. Absolute binding energies are available in the SI.

The hypothesis of catalyst activation through purely thermodynamic control considered with the relative binding energies from Table 1 suggests that most fumarate complexes (except for **2**) would be as inactive as complex **1** in reductive coupling reactions. Regardless, the increased steric bulk of the fumarates compared to **1** and variations in electronics of the aryl groups of **7-10** provided a significant range of binding energies. Therefore, this set could be used to better understand the relationship between fumarate binding and reactivity, and we experimentally tested a representative set of the compounds evaluated by computation. The model coupling reaction (Figure 3, top) was performed for representative precatalysts and monitored by ^{19}F NMR. Across the catalyst series **1-2** and **5-10**, all of the tested fumarate complexes except for catalyst **10** were found to be more active than the parent dimethyl fumarate complex **1** (see SI). Figure 3 shows that the rates and conversions were highest for those catalysts that possessed the bulkiest fumarate substituents (**2**, **6**, **7**).

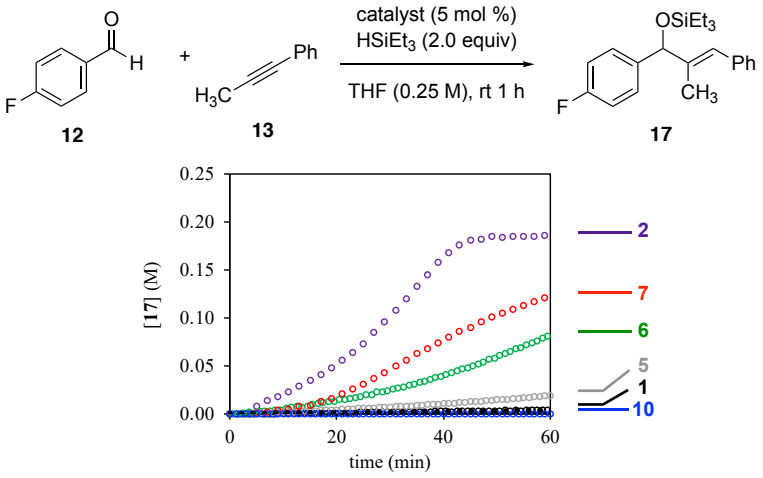

Figure 3. Reaction progression plots for select catalysts using ^{19}F NMR. Catalysts **2**, **7**, and **6** showed the most activity (see Figure 2 for structures).

The reactivity ordering in Figure 3 showed no clear relationship to the binding affinities detailed in Table 1. While the most reactive catalyst **2**, which possesses a di-(*t*-butyl) fumarate ligand, also has the most favorable exchange energy for the **14** to **15** conversion, other complexes such *o*-tol precatalyst **7** exhibited excellent catalytic reactivity at room temperature, despite having a fumarate binding affinity that

is too endergonic to undergo the **14** to **15** exchange under the reaction conditions (>14 kcal/mol above that of **1**). This means that if ligand exchange were a necessary step for catalyst activation, **7** should be completely inactive.

In addition to the precatalysts of Table 1, smaller carbenes such as the *i*-Pr-BAC cyclopropenylidene ligands were of interest to our group, as they have proven unique in related applications.[11] Catalyst **11**, however, was air stable but unreactive in aldehyde-alkyne reductive couplings. Unlike catalyst **7**, catalyst **11** was found to have a weaker fumarate binding energy that was 4.2 kcal/mol uphill of catalyst **1**. The inactivity of **11**, despite having the same fumarate as activate catalyst **7**, indicated that catalyst activity is not solely dependent on fumarate identity, but may also be affected by the interplay between the NHC ligand and the fumarate ligand.

The above results indicate that ligand exchange is probably not the mechanism of catalyst activation for catalysts such as **7**. Based on this information, we propose an alternative hypothesis: a chemical activation event is responsible for converting the precatalyst into the active catalyst. In other words, the fumarate in **7** and other precatalysts must be consumed through a chemical transformation of the π-acidic ligand prior to catalysis.

Mechanism for Catalyst Activation

We set out to test the hypothesis of ligand consumption by identifying the fate of the fumarate in the activation process. Specifically, we examined reactions with an elevated catalyst loading to allow the fate of the fumarate ligand to be tracked. Precatalyst **7** is readily prepared from $Ni(COD)_2$, IMes, and di-(*o*-tolyl) fumarate, it possesses excellent stability and reactivity, and its structure (Figure 4) is analogous to previously reported catalyst **2**. In using 50 mol % loading of catalyst **7** in the three-component coupling of 4-fluorobenzaldehyde, 1-phenyl propyne, and triethylsilane, product **18** was isolated. **18** might result from a four-component reductive cycloaddition including the di-(*o*-tolyl) fumarate from the nickel catalyst, and byproduct **19** was observed by GCMS analysis (Scheme 1). The process resembles Et_3B-mediated reductive

cycloaddition involving enoates, alkynes, and aldehydes,[12] but has not been observed or proposed as a mechanism for catalyst activation. Given the complexity and uncertain mechanism of the formation of byproduct **18**, we turned to computational reaction pathway evaluation tools to provide a clear explanation for these phenomena.

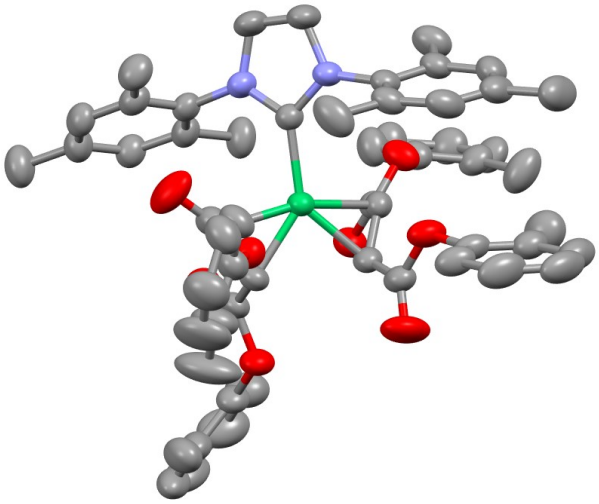

Figure 4. ORTEP diagram of complex **7** with thermal ellipsoids at 50 % probability. Hydrogen atoms are omitted for clarity.

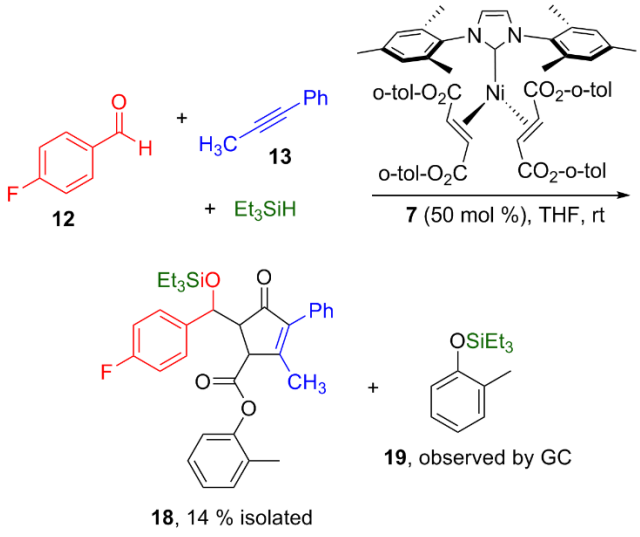

Scheme 1. Generation of products **18** and **19** in an activation pathway for catalyst **7.**

Based on analogy to our prior studies, we envisioned that **18** might derive from metallacycle **20** via oxidative cyclization of a bound fumarate ligand with an alkyne (Scheme 2). The formation of metallacycle **20** could proceed through an "aldol first" pathway[12b] involving direct addition of aldehyde to the nickel enolate of **20** to generate nickel aldolate **21**. Alternatively, a "ketene first" pathway[12c] involving aryloxy elimination from the nickel ester enolate moiety of **20** could generate ketene intermediate **22**. In either case, a cascade four-component coupling pathway combining a fumarate ligand, aldehyde, alkyne, and silane would afford products **18** and **19** while sequestering the fumarate. Once sequestered, the more active form of the catalyst would be available *in situ*. As this cascade process was predicted by computation to be essential for catalyst activation based on the energetic cost of ligand exchange, we set out to better understand the nature of the catalyst activation pathway.

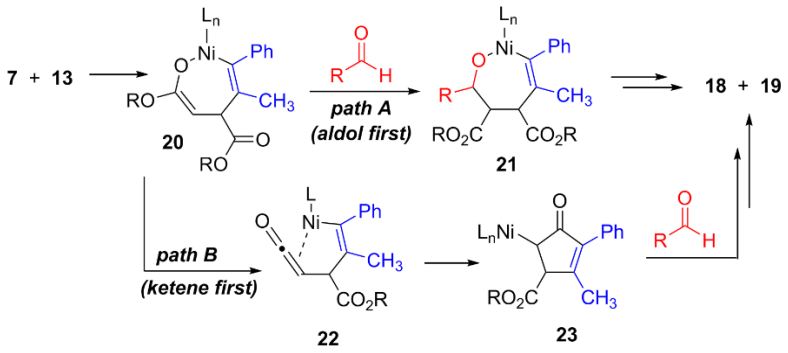

Scheme 2. Possible mechanisms for catalyst activation, leading to observed byproducts **18** and **19** (see Scheme 1).

The mechanistic details of the "aldol-first" (path A) and "ketene-first"(path B) pathways involving catalysts **7** and **11** were revealed using quantum chemical simulations (see computational details). In Figure 5, the free energy surfaces of these mechanisms for IMes catalyst **7** (pathways shown in blue and turquoise, labeled as IMes) and BAC catalyst **11** (pathways shown in red and pink, labelled as BAC) are shown. In path A (dark colors) 5-membered metallacycle **I** rotates to isomer **II**, and then isomerizes to η^3 bound **III-A** (**TS-II-A**). Complex **III-A** then isomerizes again (**TS-III-A**) to 7-membered metallacycle **IV-A**.

Alternatively, in path B (light colors), isomer **II** extrudes a unit of aryloxide (**TS-II-B**), to create ketene complex **III-B**. The ketene species can then cyclize (**TS-III-B**) to carbocyclic species **IV-B**.

To determine whether a given catalyst goes through activation path A or B, the highest energy transition states of both pathways need to be compared. In the case of catalyst **7**, with an IMes ligand, the transition state for ketene elimination (**IMes-TS-II-B**, 22.0 kcal/mol) in path B is significantly higher in energy than the highest energy transition state in path A (**IMes-TS-II-A**, 15.1 kcal/mol), which suggests that catalyst **7** undergoes activation via path A.

Intriguingly, BAC-ligated catalyst **11** has a barrier for ketene elimination (**BAC-TS-II-B**, 13.4 kcal/mol) that is significantly lower than the corresponding barrier for IMes-TS-II-B for catalyst **7**. Additionally, the barrier for isomerization from η^3 bound **BAC-III-A** (**BAC-TS-III-A**, 19.5 kcal/mol) is moderately higher than the corresponding barrier for **7** (**IMes-TS-III-A**, 13.9 kcal/mol). Taken together, the larger barrier height of **BAC-TS-III-A** (19.5 kcal/mol) compared to **BAC-TS-II-B** (13.4 kcal/mol**)** indicates that catalyst **11** prefers to undergo catalyst activation through path B.

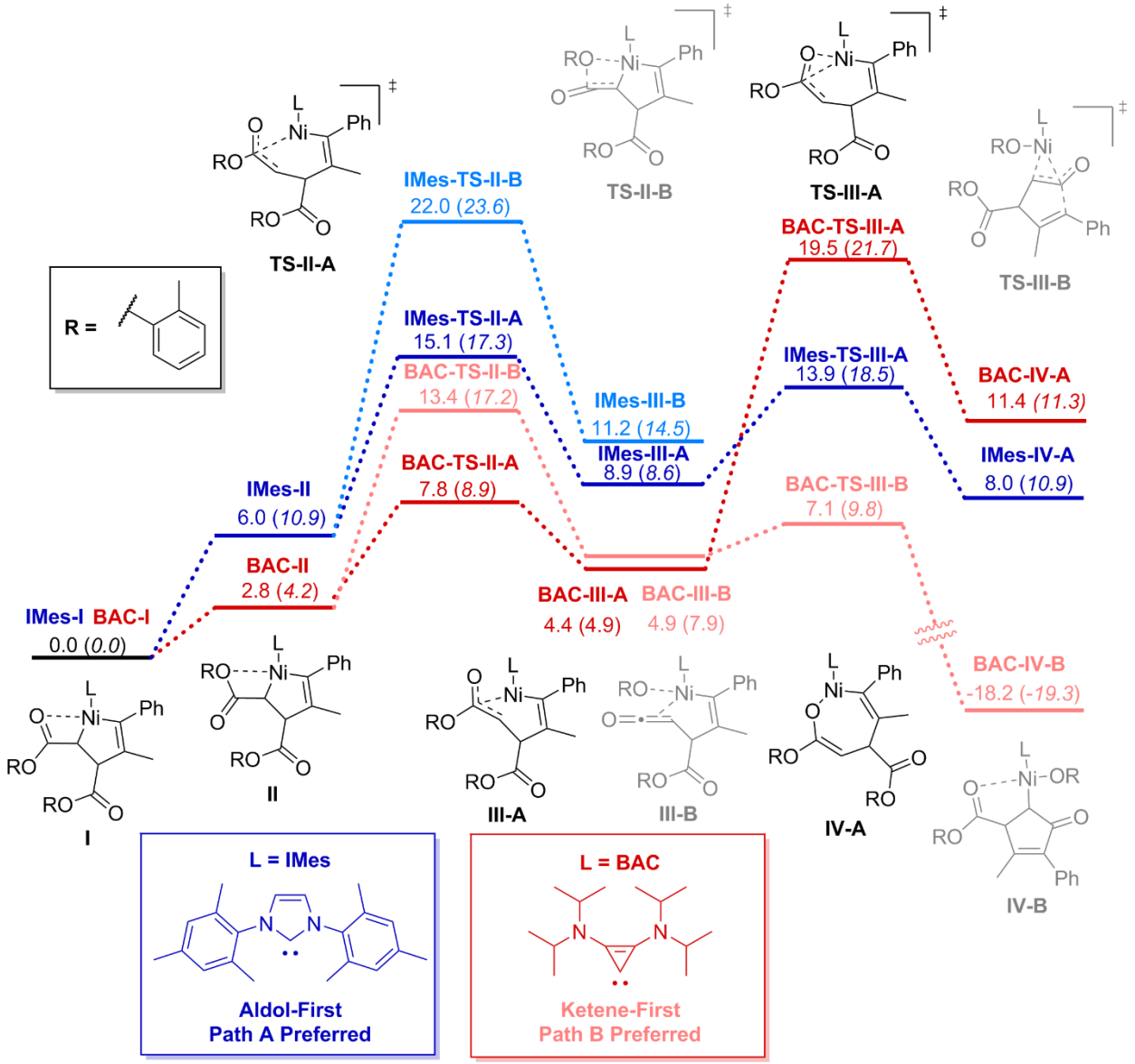

Figure 5. Free energy profile for initiation of nickel BAC and IMes complexes with di-(*o*-tolyl) fumarate. The catalyst activation sequence of BAC catalyst **11** is shown in red and in pink. The catalyst activation sequence of IMes catalyst **7** is shown in blue and turquoise. Free energies and enthalpies from ωB97X-D3/cc-pVTZ/THF are listed in kcal/mol, and enthalpy values are listed in italics. The darker colors (red, blue, and black) represent aldol-first (path A). The lighter colors (pink, turquoise, and gray) represent ketene-first (path B).

The above analysis suggests that the fumarate ligands of IMes precatalyst **7** and BAC precatalyst **11** react via different mechanisms. With this knowledge in hand, we then hypothesized that this difference can explain why **7** is a competent catalyst, but **11** is not. To evaluate this hypothesis, we followed the progression of path A in **7** and path B in **11** along the free energy surface.

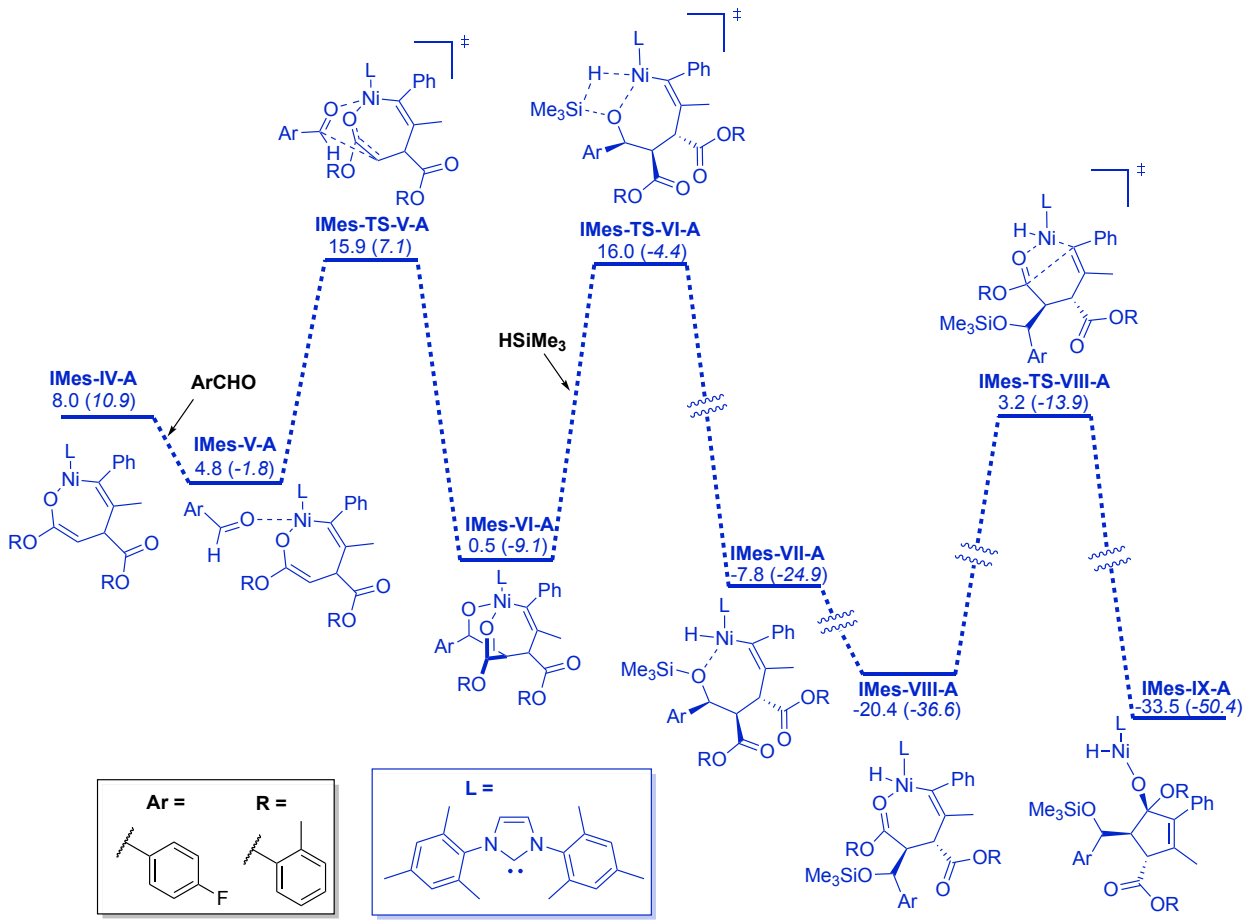

Figure 6. Free energy surface for aldol-first activation pathway of catalyst **7**. Aldol addition, hydrosilylation, and carbocyclization are shown. Free energies and enthalpies from ωB97X-D3/cc-pVTZ/THF are listed in kcal/mol, and enthalpy values are listed in italics.

In the case of catalyst **7**, path A provides a means to release a potential active catalyst. Figure 6 details the pathway for catalyst release. Seven-membered metallacycle **IMes-IV-A** can ligate to an aldehyde (**IMes-V-A**, Figure 5), and can then undergo an aldol reaction (**IMes-TS-V-A**) to yield complex

IMes-VI-A. After aldol addition, complex **IMes-VI-A** can be subsequently hydrosilylated (**IMes-TS-VI-A**), to yield complex **IMes-VII-A**, which can rearrange to complex **IMes-VIII-A**. Carbocyclization can then occur (**IMes-TS-VIII-A**, 3.2 kcal/mol), leading to nickel alkoxide species **IMes-IX-A**. This compound can easily extrude an alkoxide to yield compound **18** and an activated catalyst.

The quantum chemical results shown in Table 1 and Figures 5 and 6 can be used to explain the competency of catalyst **7** in coupling of **12** and **13.** Despite simple ligand exchange being thermodynamically unfeasible, catalyst **7** is competent in the production of allylic alcohol **17**. This implies the catalyst activation route involves consumption of the fumarate, and the catalytic activity is predicated on the formation of a byproduct such as **18** (Scheme 1). This observation motivated us to experimentally isolate compound **18** to provide a test of the fumarate consumption hypothesis. A feasible reaction pathway leading to **18** is outlined in Figures 5 and 6.

In short, catalyst **7** is competent because it can undergo a reaction that removes its (strongly bound) fumarates from solution. This observation also provides a putative reason as to why BAC catalyst **11** is incompetent in similar reductive couplings to form **12** or **13**. Computational investigation of the activation pathways for **14** suggest that a ketene-first path is preferred, in contrast to the aldol-first path preferred by **11**. As a result of this change, catalyst **11** is can form highly stabilized complex **BAC-IV-B** (Figure 5). Notably, the presence of a proximal ester moiety in the carbocycle stabilizes the complex through direct coordination of the ester to the nickel center. By occupying a coordination site, the proximal ester inhibits the coordination of an aldehyde that is possible in the previously reported enoate chemistry.[12a]

Conclusions

In summary, we introduce a new Ni(0) catalyst (**7**) complexed with IMes and two stabilizing di-(*o*-tolyl) fumarate ligands, and we demonstrate it to be a competent catalyst in the reductive coupling of aldehydes and alkynes using silanes as the terminal reductant. The catalyst is easily prepared and handled, while undergoing rapid catalyst activation under mild reaction conditions. Computational study of a panel

of catalysts that range in stability and catalyst activity illustrated that simple dissociation of fumarate ligand was unlikely to serve as the catalyst activation step, as the thermodynamics of ligand exchange are uncorrelated with catalyst activity. Instead, consumption of the fumarate through a cascade cycloaddition process involving the reaction components was identified as a likely pathway for catalyst activation. Computational studies elucidated the operative mechanism for the catalyst activation step and provided a predictive model for explaining the divergent reactivity of catalysts that possess similar structures but that undergo different activation mechanisms. This work continues to advance the development of highly active and well-defined Ni(0) catalysts that provide improvements in stability and ease of handling over the corresponding structures obtained through *in situ* catalyst preparations.

Acknowledgements

PMZ thanks the NIH (R35-GM-128830) and JM thanks the National Science Foundation (CHE-1954939) for support for this research. Dr. Jeff Kampf (University of Michigan) is kindly acknowledged for the X-ray crystallographic analysis.

References

1. (a) Montgomery, J., Organonickel Chemistry. In *Organometallics in Synthesis, Fourth Manual*, Lipshutz, B. H., Ed. John Wiley & Sons, Inc.: Hoboken, N. J. , 2013; pp 319-428; (b) Montgomery, J., Nickel-Catalyzed Reductive Cyclizations and Couplings. *Angew. Chem. Int. Ed.* **2004,** *43*, 3890-3908; (c) Tasker, S. Z.; Standley, E. A.; Jamison, T. F., Recent Advances in Homogeneous Nickel Catalysis. *Nature* **2014,** *509*, 299-309; (d) Everson, D. A.; Weix, D. J., Cross-Electrophile Coupling: Principles of Reactivity and Selectivity. *J. Org. Chem.* **2014,** *79*, 4793-4798; (e) Poremba, K. E.; Dibrell, S. E.; Reisman, S. E., Nickel-Catalyzed Enantioselective Reductive Cross-Coupling Reactions. *Acs Catalysis* **2020,** *10*, 8237-8246; (f) Rosen, B. M.; Quasdorf, K. W.; Wilson, D. A.; Zhang, N.; Resmerita, A. M.; Garg, N. K.; Percec, V., Nickel-Catalyzed Cross-Couplings Involving Carbon-Oxygen Bonds. *Chem. Rev.* **2011,** *111*, 1346-1416; (g) Zuo, Z.; Ahneman, D. T.; Chu, L.; Terrett, J. A.; Doyle, A. G.; MacMillan, D. W. C., Merging Photoredox with Nickel Catalysis: Coupling of Alpha-Carboxyl Sp(3)-Carbons with Aryl Halides. *Science* **2014,** *345*, 437-440.

2. (a) Shields, J. D.; Gray, E. E.; Doyle, A. G., A Modular, Air-Stable Nickel Precatalyst. *Org. Lett.* **2015,** *17*, 2166-2169; (b) Standley, E. A.; Jamison, T. F., Simplifying Nickel(0) Catalysis: An Air-Stable Nickel Precatalyst for the Internally Selective Benzylation of Terminal Alkenes. *J. Am. Chem. Soc.* **2013,** *135*, 1585-1592; (c) Lavoie, C. M.; MacQueen, P. M.; Rotta-Loria, N. L.; Sawatzky, R. S.; Borzenko, A.; Chisholm, A. J.; Hargreaves, B. K. V.; McDonald,

R.; Ferguson, M. J.; Stradiotto, M., Challenging Nickel-Catalysed Amine Arylations Enabled by Tailored Ancillary Ligand Design. *Nature Communications* **2016,** *7*, 11073; (d) Park, N. H.; Teverovskiy, G.; Buchwald, S. L., Development of an Air-Stable Nickel Precatalyst for the Amination of Aryl Chlorides, Sulfamates, Mesylates, and Triflates. *Org. Lett.* **2014,** *16*, 220-223; (e) Magano, J.; Monfette, S., Development of an Air-Stable, Broadly Applicable Nickel Source for Nickel-Catalyzed Cross-Coupling. *ACS Catalysis* **2015,** *5*, 3120-3123; (f) MacQueen, P. M.; Tassone, J. P.; Diaz, C.; Stradiotto, M., Exploiting Ancillary Ligation to Enable Nickel-Catalyzed C-O Cross-Couplings of Aryl Electrophiles with Aliphatic Alcohols. *J. Am. Chem. Soc.* **2018,** *140*, 5023-5027.

3. Todd, D. P.; Thompson, B. B.; Nett, A. J.; Montgomery, J., Deoxygenative C-C Bond-Forming Processes Via a Net Four-Electron Reductive Coupling. *J. Am. Chem. Soc.* **2015,** *137*, 12788-12791.

4. Nett, A. J.; Zhao, W. X.; Zimmerman, P. M.; Montgomery, J., Highly Active Nickel Catalysts for C-H Functionalization Identified through Analysis of Off-Cycle Intermediates. *J. Am. Chem. Soc.* **2015,** *137*, 7636-7639.

5. Mennen, S. M.; Alhambra, C.; Allen, C. L.; Barberis, M.; Berritt, S.; Brandt, T. A.; Campbell, A. D.; Castañón, J.; Cherney, A. H.; Christensen, M.; Damon, D. B.; Eugenio de Diego, J.; García-Cerrada, S.; García-Losada, P.; Haro, R.; Janey, J.; Leitch, D. C.; Li, L.; Liu, F.; Lobben, P. C.; MacMillan, D. W. C.; Magano, J.; McInturff, E.; Monfette, S.; Post, R. J.; Schultz, D.; Sitter, B. J.; Stevens, J. M.; Strambeanu, I. I.; Twilton, J.; Wang, K.; Zajac, M. A., The Evolution of High-Throughput Experimentation in Pharmaceutical Development and Perspectives on the Future. *Organic Process Research & Development* **2019,** *23*, 1213-1242.

6. Clement, N. D.; Cavell, K. J.; Ooi, L.-l., Zerovalent N-Heterocyclic Carbene Complexes of Palladium and Nickel Dimethyl Fumarate: Synthesis, Structure, and Dynamic Behavior. *Organometallics* **2006,** *25*, 4155-4165.

7. Nett, A. J.; Canellas, S.; Higuchi, Y.; Robo, M. T.; Kochkodan, J. M.; Haynes, M. T.; Kampf, J. W.; Montgomery, J., Stable, Well-Defined Nickel(0) Catalysts for Catalytic C-C and C-N Bond Formation. *ACS Catal.* **2018,** *8*, 6606-6611.

8. Berini, C.; Winkelmann, O. H.; Otten, J.; Vicic, D. A.; Navarro, O., Rapid and Selective Catalytic Oxidation of Secondary Alcohols at Room Temperature by Using (N-Heterocyclic Carbene)-Ni-0 Systems. *Chem.-Eur. J.* **2010,** *16*, 6857-6860.

9. (a) Nattmann, L.; Saeb, R.; Noethling, N.; Cornella, J., An Air-Stable Binary Ni(0)-Olefin Catalyst. *Nature Catalysis* **2020,** *3*, 6-13; (b) Tran, V. T.; Li, Z. Q.; Apolinar, O.; Derosa, J.; Joannou, M. V.; Wisniewski, S. R.; Eastgate, M. D.; Engle, K. M., Ni(Cod)(Dq): An Air-Stable 18-Electron Nickel(0)-Olefin Precatalyst. *Angew. Chem. Int. Ed.* **2020,** *59*, 7409-7413.

10. (a) Iglesias, M. J.; Blandez, J. F.; Fructos, M. R.; Prieto, A.; Alvarez, E.; Belderrain, T. R.; Nicasio, M. C., Synthesis, Structural Characterization, and Catalytic Activity of Iprni(Styrene)(2) in the Amination of Aryl Tosylates. *Organometallics* **2012,** *31*, 6312-6316; (b) Wu, J. G.; Faller, J. W.; Hazari, N.; Schmeier, T. J., Stoichiometric and Catalytic Reactions of Thermally Stable Nickel(0) Nhc Complexes. *Organometallics* **2012,** *31*, 806-809; (c) Elsby, M. R.; Johnson, S. A., Nickel-Catalyzed C-H Silylation of Arenes with Vinylsilanes: Rapid and Reversible Beta-Si Elimination. *J. Am. Chem. Soc.* **2017,** *139*, 9401-9407.

11. (a) Malik, H. A.; Sormunen, G. J.; Montgomery, J., A General Strategy for Regiocontrol in Nickel-Catalyzed Reductive Couplings of Aldehydes and Alkynes. *J. Am. Chem. Soc.* **2010,** *132*, 6304-6305; (b) Kuchenbeiser, G.; Donnadieu, B.; Bertrand, G., Stable

Bis(Diisopropylamino)Cyclopropenylidene (Bac) as Ligand for Transition Metal Complexes. *J. Organomet. Chem.* **2008,** *693*, 899-904.
12. (a) Jenkins, A. D.; Robo, M. T.; Zimmerman, P. M.; Montgomery, J., Nickel-Catalyzed Three-Component Cycloadditions of Enoates, Alkynes, and Aldehydes. *J. Org. Chem.* **2020,** *85*, 2956-2965; (b) Jenkins, A. D.; Herath, A.; Song, M.; Montgomery, J., Synthesis of Cyclopentenols and Cyclopentenones Via Nickel-Catalyzed Reductive Cycloaddition. *J. Am. Chem. Soc.* **2011,** *133*, 14460-14466; (c) Ohashi, M.; Taniguchi, T.; Ogoshi, S., Nickel-Catalyzed Formation of Cyclopentenone Derivatives Via the Unique Cycloaddition of Alpha,Beta-Unsaturated Phenyl Esters with Alkynes. *J. Am. Chem. Soc.* **2011,** *133*, 14900-14903.

Synopsis TOC